Flow Separation and Wake of the Common Research Model at Low Mach Numbers

Maximilian Ehrle
Andreas Waldmann
Thorsten Lutz
Ewald Krämer
GERMANY

ehrle@iag.uni-stuttgart.de

ABSTRACT

The present investigation focuses on beginning stall at moderate angles of attack at the NASA Common Research Model and represents a natural follow-up to post-stall studies at high angles of attack in previous work in the authors' working group. Flow separation characteristics are analysed at three angles of attack by three different hybrid RANS/LES models, namely IDDES, DDES and AZDES. The wing pressure distributions are compared to experimental data from the European Strategic Wind Tunnels Improved Research Potential (ESWI^{RP}) project. All three models show fully attached flow at α =10°. For α =12° a spanwise variation of separation characteristics can be observed between the models while all models overestimate flow separation. Nevertheless, IDDES yields better agreement in comparison to experimental data at this angle of attack but still overpredicts flow separation. For an angle of attack of α =14° all three models show similar results but still overestimate the area of flow separation in comparison to experimental data.. The differences could be traced back to different filter width definitions of IDDES and the other two models which lead to a faster breakup of turbulent structures and a smaller recirculation area in the IDDES case.

1.0 INTRODUCTION

Beginning flow separation on transport aircraft limits their flight performance and represents a safety-critical aspect. A correct prediction of the stalling characteristics of the wing, including the formation of vortices and turbulent structures, which propagate downstream in the wake and may induce loads on the empennage, is essential for structural integrity and control. Nevertheless, the prediction of beginning flow separation still poses significant difficulties to numerical methods to properly predict the correct angle of attack at which stall occurs, separation position and the development of separation induced turbulence. Therefore, evaluation, development and selection of appropriate numerical methods for the simulation of aircraft aerodynamics at the borders of the flight envelope are of special interest. A more accurate prediction and understanding of safety critical aerodynamic phenomena allows a deeper insight into flow physics and interactions which may occur at stall conditions. These pursuits are driven by the need to better characterize the behavior of passenger aircraft far from their design conditions, in situations that are difficult to predict via wind tunnel experiments or flight tests.

Post stall wake and high-speed stall of transport aircraft were investigated in several studies of the authors' working group, including the typical airliner cruise conditions around the transonic design Mach number [5,8] as well as high angle of attack situations at low speed stall [8,16,17]. As the aforementioned studies showed superior results of hybrid RANS/LES models in comparison to unsteady RANS in terms of the extent of the separated wake as well as its turbulent content, these models shall be applied in the following. The present work focuses on beginning flow separation at flight relevant Reynolds numbers, low speed and moderate angles of attack, as indicated by the red circle in Figure 3-2. Consequently it represents a natural follow-up to the studies at high angle of attack and fully separated flow. Fundamental characteristics of stall

behavior and development of turbulence in vicinity of the separation position as well as above the wing surface shall be investigated and give insight into the physical mechanisms of stall at swept wings.

Common shortcomings of different DES-type methods include modelled stress depletion and grid-induced separation. Flows involving smooth surface separation, which might occur at moderate angles of attack, are more sensitive to these issues than the geometry-defined leading edge separation that could be observed at higher angles of attack. For this reason, a comparison of simulations at these challenging conditions using the DDES (Delayed Detached Eddy Simulation)[14] and IDDES (Improved Delayed Detached Eddy Simulation)[12] approaches as well as the in-house developed AZDES (Automated Zonal DES)[2,8] method for TAU [11] is performed. While DDES and IDDES rely on a delay function in order to prevent early switching from RANS turbulence to resolved LES content, the AZDES approach allows additional shielding of the attached flow regions by enforcing RANS in locations specified by the user via solution-based variables. This approach was validated in high speed stall conditions [2,8]. The present work provides insight in previous research on the CRM stall and presents a short summary of flow separation on swept wings in the following section. Subsequently the computational setup including simulation models and grid is described. The main section presents the simulation results as well as their interpretation and is concluded by a summary and outlook.

1.1 Flow separation and wake of transport aircraft

The NASA Common Research Model (CRM) [15], which is investigated in the following has established itself as a widely used configuration for studies focusing on contemporary aircraft designs. Within the scope of numerical investigations at this transport aircraft [8] it was possible to observe flow separation beginning at an angle of attack of 10° at the wing tip, which extends to the entire wing as the angle of attack increases. Stall at high angles of attack at the CRM has been extensively studied by Waldmann et al.[16,17]. Furthermore, Waldmann et al.[16] showed that wake physics could be resolved for these conditions using scale-resolving methods such as Detached Eddy Simulation (DES) leading to reliable results of aerodynamic coefficients. Unsteady RANS methods, on the other hand, are capable of reliably handling flow without separation until $\alpha \approx 10^{\circ}$. As shown in the same work, the post-stall wake is dominated by the shear layers emanating from the leading edge and trailing edge of the wing, whose destabilization and collapse determine the shape and size of the recirculation region. This flow exhibits bluff body-like characteristics, with a large wake undulating in the manner of a vortex street. This meandering motion contains a significant part of the total fluctuation energy in the wake and takes place in a Strouhal number range between 0.2 and 0.6, which agrees well with the supercritical regime described for unswept airfoils by Huang and Lin [4]. This showed that these simulations allow insight into the dynamics of the wake due to their significant spatial and temporal resolution. The high angles of attack described above facilitate the use of DES-type methods, as the separation is triggered directly at the wing leading edge by the geometrical shape and extends over the entire wing span. Moderate α values between the onset of separation and the fully separated post-stall conditions pose the additional difficulty of a possibly varying separation location, which is not necessarily fixed by geometrical shape. Pressure driven smooth surface separation might occur, which still represents one major challenge for computational fluid dynamics [7]. In addition, spanwise flow effects on swept wings may lead to variations of separation characteristics or possible unsteady reattachment phenomena that make a proper representation of the flow physics even more difficult. Flow separation on swept wings shows, in comparison to airfoils and unswept wings, different characteristics concerning separation behavior. As Harper and Maki [3] already discussed in the 1960s, wing sweep might result in a shifting of flow separation from the trailing edge to the leading edge. Furthermore, they showed that an increase in angle of attack during growing flow separation leads to an inboard movement of the tip vortex which results in an increased drag. In addition, a fast shift of the separation position from the trailing to the leading edge might be induced by the characteristic strong suction peak of transonic airfoils such as the one used at the CRM.

2.0 COMPUTATIONAL SETUP

The flow conditions are chosen according to the ESWI[RP] wind tunnel measurements in the European Transonic Windtunnel (ETW) (run 316) [8] including a 2.7% scale model of the NASA CRM, a Reynolds number based on the mean chord (MAC = 0.189m) of 11.6 Mio and a Mach number of 0.25. The angles of attack on which this work focuses are 12° and 14°. A detailed description of the model can be found in Vassberg et al.[15]. The wind tunnel campaign is described by Lutz et al.[8]. The computational grid corresponds to the hybrid grid described in detail in [17] without a fully structured wake, but with an integrated hexahedral block on the wing suction side and in vicinity of the trailing edge in order to resolve flow physics in the stall region and beginning wake. The boundary layer mesh consists of prisms, mainly at the fuselage, as well as hexahedra at the wing and horizontal tailplane surfaces. The mesh resolution on the wall is chosen in such a way that y^+ of the first gridpoint is smaller than one on the entire airplane surface.

The deformation of the wind tunnel model was taken into account by deforming the grid according to wind tunnel data. Because this work focuses on separation at the wing, the wake was filled with tetrahedra in order to save gridpoints and computational cost. The boundary layer mesh as well as a slice though the structured block on the wing suction side are shown in Figure 3-1. Overall, the grid contains a total of 38 million gridpoints. A summary of simulation parameters is given in Table 3-1.

Table 3-1: Flow conditions and simulation runs

MAC	M_∞	Re_∞	α
0.189144m	0.25	$11.6 \cdot 10^6$	$12° - 14°$

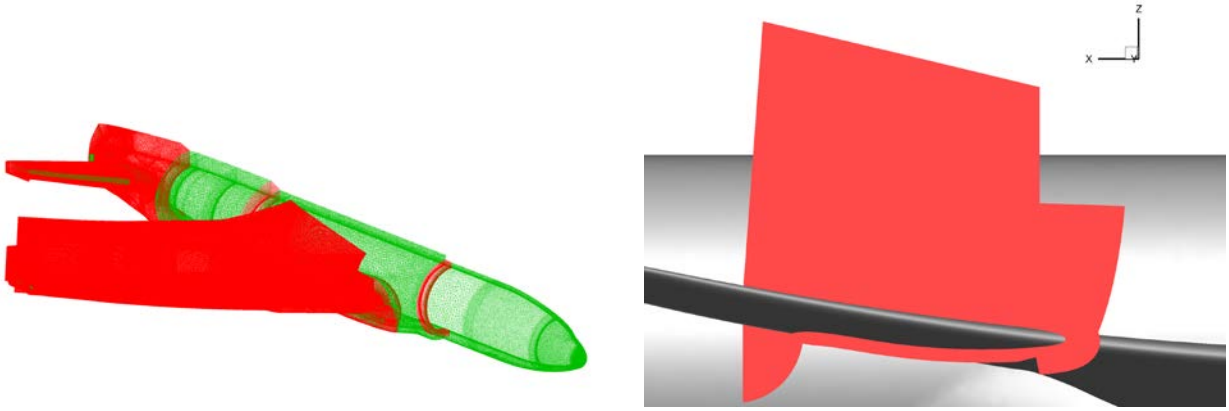

Figure 3-1: CRM boundary layer mesh and hexahedral blocks (prisms green, hexahedra red) and a slice through the structured hexahedra block at 50% semi-span

All simulations in this work were performed with the unstructured finite volume solver TAU [11] version 2018.1.0 by DLR. A central differencing scheme provides second order accuracy for the convective terms. Matrix-valued artificial dissipation with low dissipation settings in scale resolving regions ($k^{(4)}$=1/1024) and standard dissipation settings in RANS regions ($k^{(4)}$=1/64) stabilizes the numerical scheme. The most recent low dissipation and low dispersion models [10] are employed in order to ensure optimum accuracy of the turbulence propagation in the scale resolving regions. As another measure to mitigate the grey area problem of hybrid RANS/LES-models, the vorticity-sensitive filter width model $\tilde{\Delta}_\omega$ according to [9] is applied. Furthermore, a first order Roe scheme is used for the convective fluxes of the turbulence equations and a LU-SGS scheme serves as linear solver. Second order temporal discretization is realized with a Backward-Euler dual time stepping scheme. The physical timestep for computations of Δt=34µs is chosen according to Waldmann et al. [16], which corresponds to 100 timesteps per convective time unit $t_\infty = MAC/u_\infty$.

Convergence acceleration is realized via a 5w multigrid cycle. The number of inner iterations is set to 100. As a consequence of the high Reynolds number, the flow is considered fully turbulent.

The hybrid RANS/LES models use the Spalart-Allmaras (SA) model in its original formulation as turbulence model[13], which showed good results in previous studies at higher angles of attack [16,17]. Steady state computations deliver the starting point for unsteady URANS simulations, which are performed subsequently as starting point for the hybrid simulations. The AZDES method requires a precursor URANS simulation, which was run over 20 $\cdot t_\infty$ leading to a representative distribution of the turbulent length scale used in the AZDES as basis for the definition of the RANS and DES zones respectively. The hybrid RANS/LES simulations in this work are performed using DDES, IDDES and AZDES models. DDES and IDDES both evolved from the original DES formulation [13] of Spalart et al. and include enhancements such as boundary layer shielding. Further information about the DDES and IDDES models can be found in Spalart et al. [14] and Shur et al.[12], respectively. The AZDES was developed for transonic flow cases with shock induced separation and transonic buffet, where conventional hybrid RANS/LES models show shortcomings such as modelled stress depletion and grid-induced separation. First applications in this flow regime were shown at the CRM [8, 2]. This method introduces a zonal, time independent shielding of the attached boundary layer based on results of a precursor URANS simulation. Similar to Zonal DES (ZDES) [1], a blending function f_a defines the RANS/LES interface. This function can be influenced by evaluating the turbulent length scale of the precursor computation, as well as by two wall distance dependent parameters. In the following a short description of the AZDES model is presented.

As first step for creating the RANS/LES zone division, f_a is set by a user defined threshold value L_c of the turbulent length scale L_t following Eq.(1). All points in the computational domain with L_t smaller L_c are consequently treated in RANS mode. If $L_t > L_c$, DES mode is activated.

$$f_a^{L_t} = \frac{1}{2}\tanh\left[8 \cdot \left(\frac{L_t}{L_c} - 1\right)\right] + \frac{1}{2} \qquad (1)$$

Close to the wall, i.e. when $d < d_{RANS}$, an additional shielding of the boundary layer can be activated, which overwrites areas of DES mode in this region. The value of f_a follows Eq.(2):

$$f_a = \frac{1}{2}\tanh\left[8 \cdot \left(\frac{d}{d_{RANS}} - 1\right)\right] + \frac{1}{2}, for\ 0 < d < d_{RANS} \quad (2)$$

The third parameter defines a wall distance, above which DES content is allowed independently of the state of flow separation. This parameter d_{DES} modifies f_a where $d > d_{DES}$:

$$f_a = \frac{1}{2}\tanh\left[8 \cdot \left(\frac{d}{d_{DES}} - 1\right)\right] + \frac{1}{2}, for\ d_{DES} < d < \infty \qquad (3)$$

In the present work, L_c and d_{DES} are set to 1% of the mean aerodynamic chord, d_{RANS} is set to 0.

3.0 RESULTS

Waldmann et al. [16] already demonstrated good agreement of DDES simulation results with experimental data for high angles of attack. The lift coefficient as well as the dimensionless frequency of wake structures agreed with the theory of unswept wings and revealed a bluff body like behavior. Figure 3-2 shows the lift coefficient of the CRM related to the angle of attack, which was determined during the ESWI[RP] campaign. Grey circles represent DDES, whereas the grey circle at α=18° indicates Waldmann et al.'s DDES result [16]. The green squares indicate IDDES results for angles of attack of 10°, 12° and 14°, blue triangles represent AZDES solutions at the respective angles of attack.

It is clearly visible that at **α** =10° all three models show good agreement to the experimental values. All three models underpredict the lift coefficient for higher angles of attack, IDDES yields the best agreement with experimental data for 12° and 14°, whereas DDES and AZDES both result in similar lower C_L values.

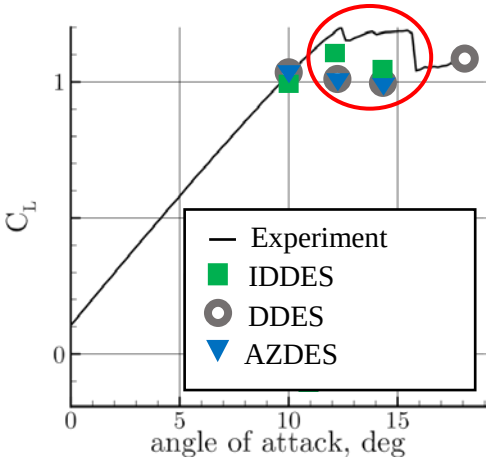

α	Exp.	$C_{L,IDDES}$	$C_{L,DDES}$	$C_{L,AZDES}$
10	1.04	0.997	1.048	1.051
12	1.19	1.11	1.03	0.993
14	1.19	1.04	0.995	0.982

Figure 3-2: CRM polar at M_∞ = 0.25, Re_∞ = 11.6 · 10^6, red circle: region of interest, lift coefficient of simulations at different angles of attack

The wind tunnel data of the pressure coefficient on the wing surface are compared to the different models' solutions in Figure 3-3 at several slices through the wing at α=12°. In the inboard area until 30% of the semi-span, all simulations fit well to experimental data and yield similar results. Between 40% and 60% semi-span, IDDES matches very well with the experiment in terms of the suction peak near the leading edge and the overall pressure distribution, whereas AZDES and DDES underestimate the suction peak. In addition, AZDES and DDES show an immediate rise of c_p in vicinity of the leading edge outboard of 40% semispan followed by a plateau of constant pressure which hints at beginning flow separation at these positions. Both AZDES and DDES underestimate the pressure level on the wing suction side downstream of x/c=0.3.

At 73% semi-span IDDES still shows good agreement with the experiment and reproduces shape and level of the pressure distribution. DDES and AZDES both underestimate the pressure, showing a plateau of constant c_p starting in vicinity of the leading edge which hints at fully separated flow at this spanwise position. At the two outboard positions IDDES shows the described signs of flow separation at the leading edge in the mean pressure distribution namely an immediate rise of c_p as well as constant c_p further downstream. DDES and AZDES show a smoother increase of pressure which matches the experimental data at 95% halfspan. IDDES leads to a lower pressure level on the wing suction side in this region.

The experimental data shows a smoother increase of pressure after the suction peak throughout the entire

wingspan, which leads to the assumption that no flow separation occurred at 12° during the experiment. Consequently, all three models seem to overestimate flow separation at α = 12°. IDDES matches best with the experiment in inboard regions while DDES and AZDES show better agreement at the wing tip.

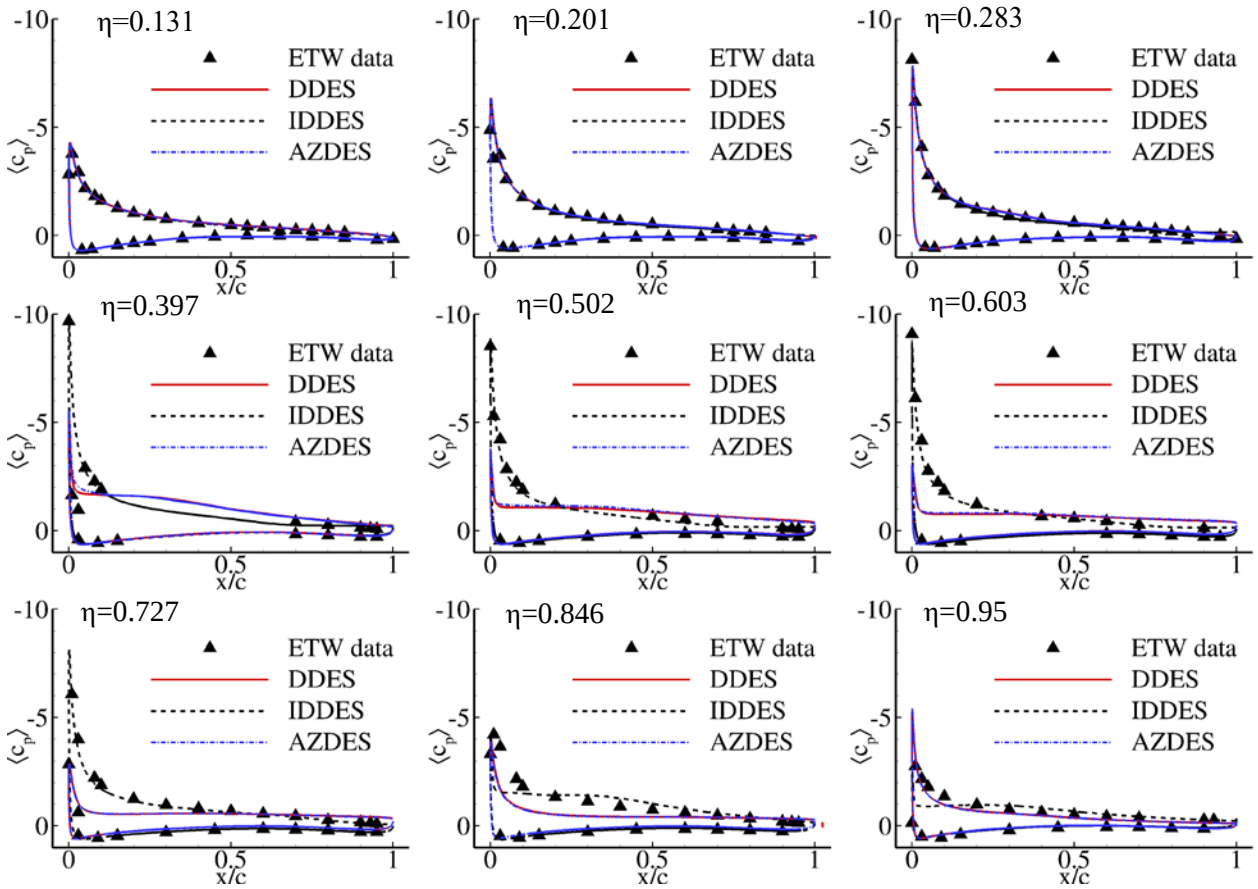

Figure 3-3: Mean pressure coefficient on the wing surface in several slices, α=12°

Figure 3-4 shows the root mean square of the pressure coefficient on the wing suction side as well as time averaged surface streamlines for IDDES, DDES and AZDES at an angle of attack of 12°. IDDES shows a surface vortex near the leading edge as well as higher pressure fluctuations in the region of 80% semi-span. In this region we already expected flow separation based on the pressure distribution of Figure 3-3. Furthermore a vortical structure in vicinity of the yehudi break in combination with trailing edge separation can be observed. DDES and AZDES show an inboard shift of the leading edge vortex as well as an increase in vortex size. The flow is separated at the leading edge between 30% and 70% of the semi-span. In the outboard wing section the separation location is shifted toward the trailing edge showing no flow separation at 95% semi-span.

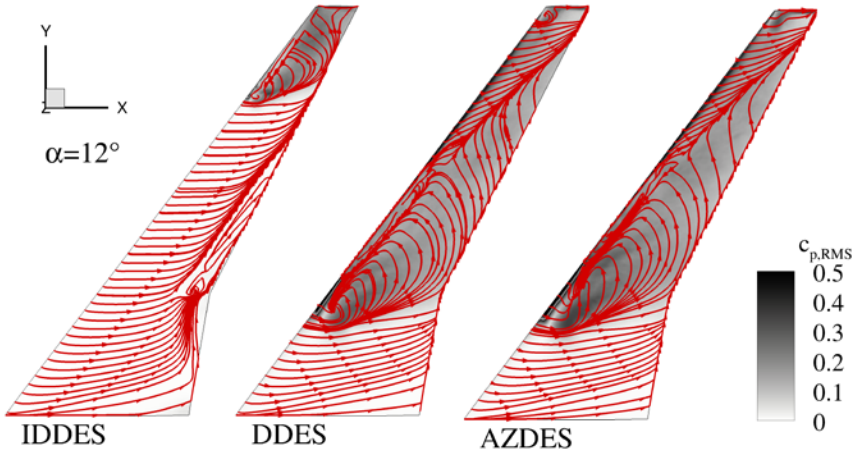

Figure 3-4: RMS of pressure coefficient on the wing suction side and surface streamlines, α=12°

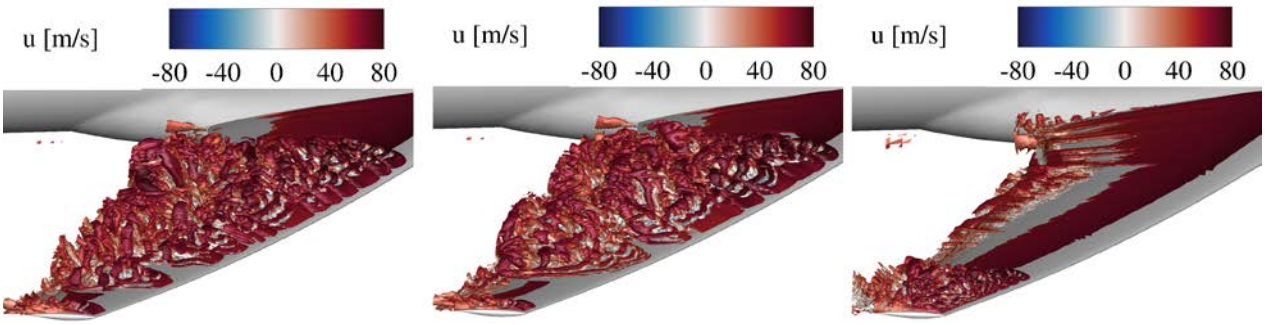

(a) AZDES (b) DDES (c) IDDES

Figure 3-5: Surfaces of λ_2 =-100000 at α=12° above the wing, colored by streamwise velocity

AZDES shows the same characteristics as DDES. In both cases, no trailing edge separation inboard of the trailing edge kink can be observed. A possible explanation for the leading edge separation in the vortex region of all three cases is the strong pressure peak of the supercritical airfoil which accelerates the movement of flow separation from the trailing edge area toward the leading edge area. Furthermore, the wing sweep might amplify this behavior by spanwise flow effects as proposed by Harper and Maki [3].

Figure 3-5 shows the development of turbulent structures on the wing suction side at α=12° by means of λ_2 isosurfaces. Besides the difference in separation size, which could already be observed in Figure 3-4, AZDES and DDES show a similar development of turbulent structures. IDDES shows a quicker development of small eddy structures directly after separation and smaller turbulent structures in the entire separation zone. These observations give rise to the question why the three different models show such a different separation behavior which causes different predictions of the lift coefficient.

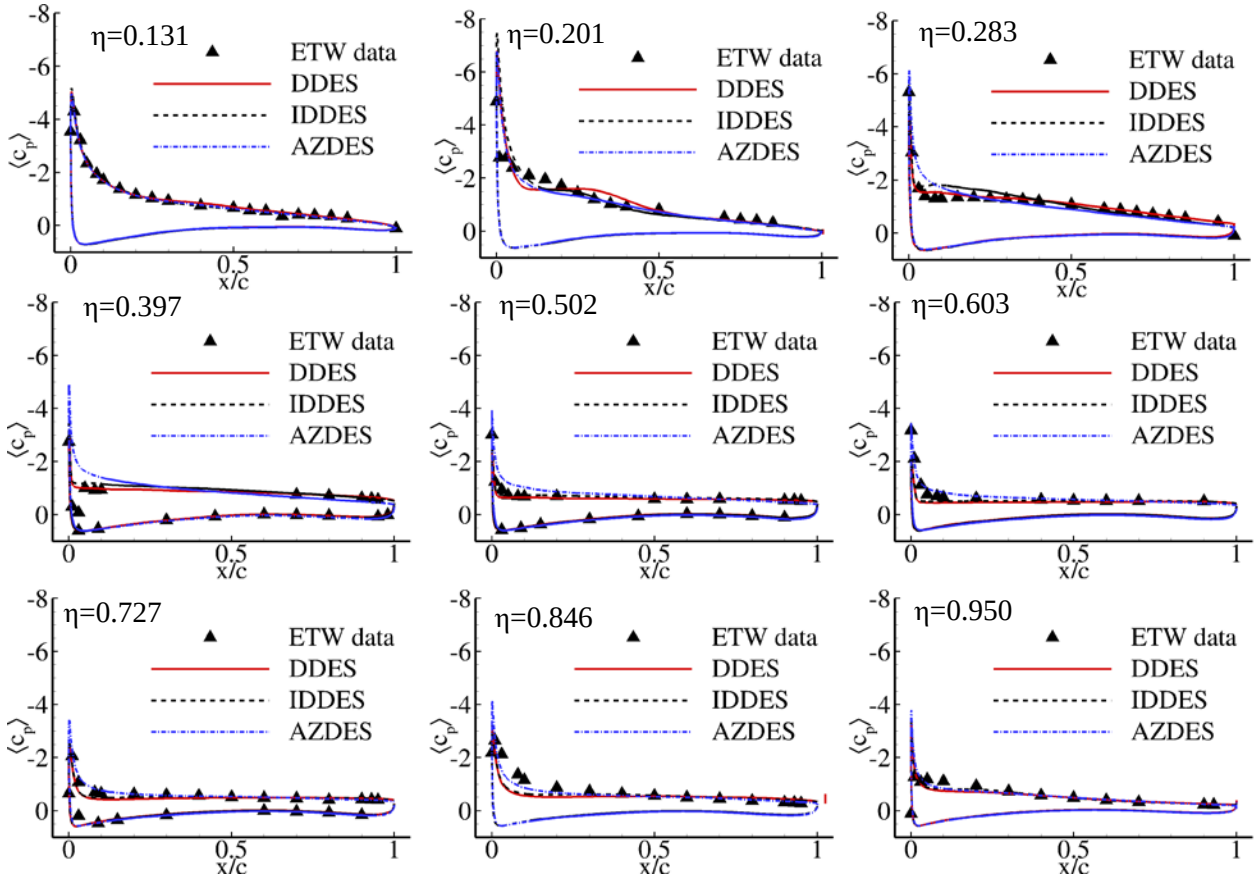

Figure 3-6: mean pressure coefficient on the wing surface in several slices, α=14°

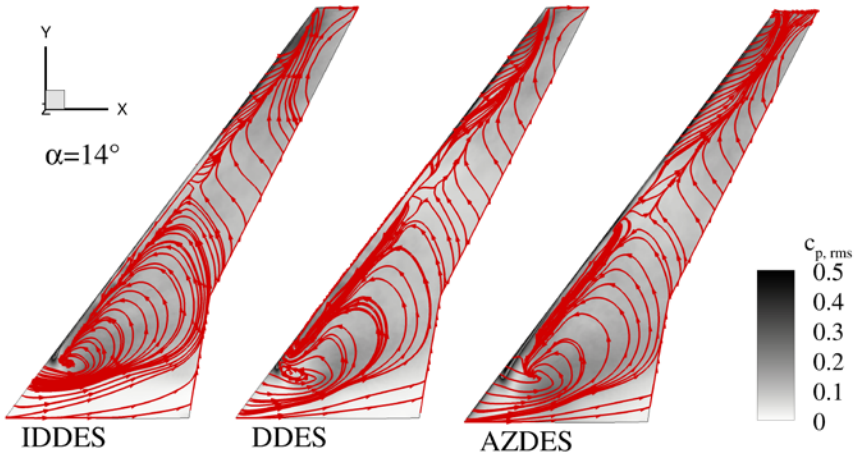

Figure 3-7: RMS of pressure coefficient on the wing suction side and surface streamlines, α=14°

Before performing a more in-depth analysis of the different models' behaviors, an analysis of flow separation at an angle of attack of 14° is performed. The mean pressure distribution in several slices on the wing surface for α=14° is shown in Figure 3-6. In this case all three simulations show a comparable behavior throughout the entire halfspan. In the wing tip region, they tend to a too early rise in pressure, which hints at overestimated flow separation. The resemblance of the flow patterns can be observed in Figure 3-7 by means of the rms of c_p as well as the surface streamlines. All three simulations show a similar streamline

distribution. The surface vortex near the leading edge that was observed in the 12° case has moved further inboard in all cases and is located at approx. 15% semi-span. The whole wing shows large recirculation areas and flow separation occurs over the entire wingspan. Furthermore, parts of the leading edge in the outboard wing section show a spanwise flow but do not seem to be separated. The λ_2 structures in Figure 3-8 confirm these observations. Near the wing tip, the separation position has moved downstream and is no longer placed directly at the leading edge in all three simulations. In addition, similarly to α=12°, IDDES shows a quicker development of small eddy structures downstream of the separation location. The better agreement of all three models with experimental data and in comparison to each other at higher angles of attack shows the good applicability of either of these models for post-stall investigations at fully separated wings.

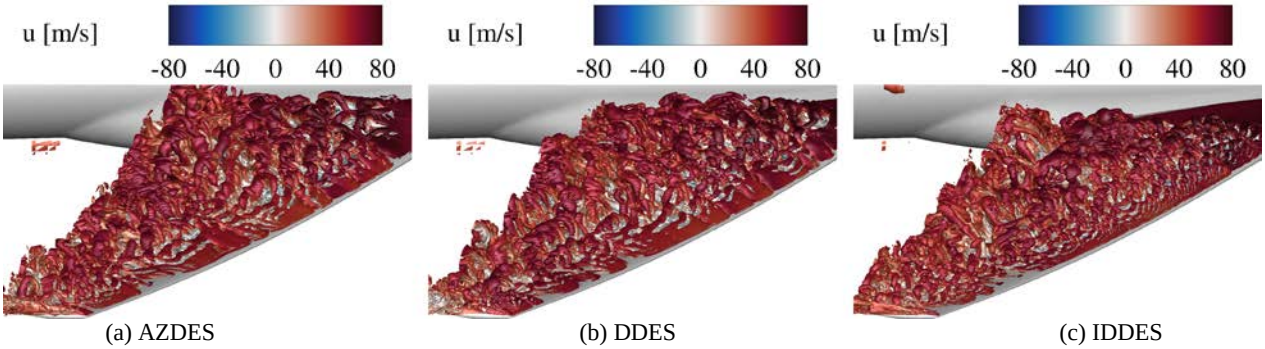

(a) AZDES (b) DDES (c) IDDES

Figure 3-8: Surfaces of λ_2 =-100000 at α=14° above the wing, colored by streamwise velocity

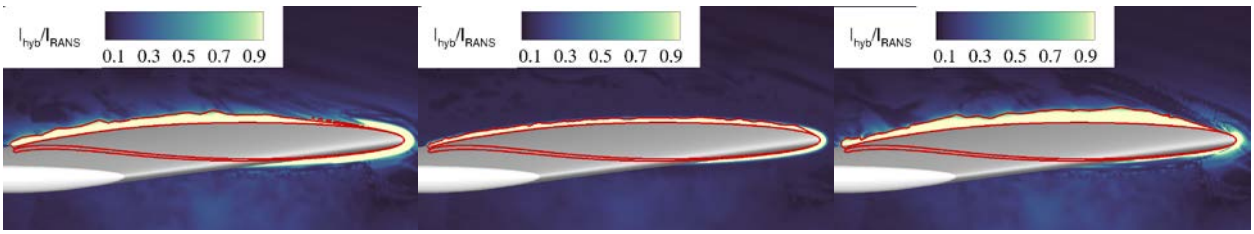

(a) AZDES (b) IDDES (c) DDES

Figure 3-9: Ratio of hybrid to RANS length scale at η =0.85, RANS zones yellow and scale resolving zones blue, lines of f_d = 0.5 in AZDES and DDES as well as f_{dt} = 0.5 in IDDES, α=12°

In order to investigate the models' differences for beginning flow separation, Figure 3-9 shows the distributions of RANS zones and scale resolving zones at α=12° in a slice of 85% semi-span. In addition, the DDES and IDDES boundary layer shielding functions are represented by red lines and show areas close to the surface which are treated in RANS mode due to these functions. RANS areas outside the red line are activated either by the user (AZDES), the grid spacing (DDES, this represents the original DES97 behavior) or different relations between grid spacing and wall distance (IDDES). As all three models show RANS behavior near the leading edge without triggered boundary layer shielding (leading edge area is located outside of the shielding area, indicated by the red line in Figure 3-9), none of the mentioned problems of modelled stress depletion and grid induced separation caused by insufficient boundary layer shielding applies. This is also an explanation for the similar behavior of AZDES and DDES as the additional shielding of AZDES is not required to protect the boundary layer from under resolved LES content. A closer look at the different models' formulation reveals a possible explanation. In DDES, the LES length scale is defined as

the product of filter width, in this case $\tilde{\Delta}_{\omega}$, a numerical constant $C_{DES} = 0.65$ and a low Re correction in the whole computational area.

In IDDES, the filter width is modified by a function of the wall distance $\Delta = \min\{\max[C_w d_w, C_w h_{max}, h_{wn}], h_{max}\}$ with $C_w = 0.15$, h_{wn} the wall normal grid step, d_w the wall distance and h_{max} the maximum cell length. In the current case, this formulation leads to a decrease of the filter width and consequently LES length scale above the wing suction side which results in an increased resolution of turbulent structures and their faster breakup finally leading to a favorable mitigation of the grey area in IDDES. This effect results in a decrease of the size of the recirculation area which is indicated in Figure 3-10 by the mean streamwise velocity in two slices through the CRM wing at an angle of attack of 14°. At 50% semi-span, DDES shows a larger recirculation area in wall normal as well as in streamwise direction in Comparison to IDDES. Furthermore, AZDES yields a decrease of wall normal extent but an increase of the streamwise extent of recirculation in comparison to IDDES. At 80% semi-span only DDES shows a significant area of negative mean velocity. In contrary, IDDES shows only small recirculation and AZDES no areas of negative streamwise velocity at all. A possible explanation for these differences in flow separation area and size of the recirculation zone is the already mentioned formation of smaller eddies in vicinity of the leading edge in the IDDES case, which can be observed in the λ_2 structures shown in Figure 3-8. These small scale structures lead to a more unstable shear layer emanating from the leading edge and accelerate the decay of turbulent structures resulting in a smaller recirculation area. This behavior also gives a possible explanation for the major difference of flow separation in the case of α=12°. A bigger separation area might change the pressure distribution of the wing, lead to a change in induced angle of attack and consequently amplify the effect and result in a further increase of separation including an inboard shift of the surface vortex.

All in all, IDDES is slightly superior in this usecase due to an effective decrease of grey area. No smooth surface separation could be observed in this case due to the effect of leading edge separation caused by the characteristics of the supercritical profile and wing sweep effects. Nevertheless, further development of hybrid models is necessary in order to be able to reproduce the stalling characteristics which were observed in the experiment. This will include further acceleration of RANS to LES transition, the use of different turbulence models, grid modifications and variation of dissipation settings.

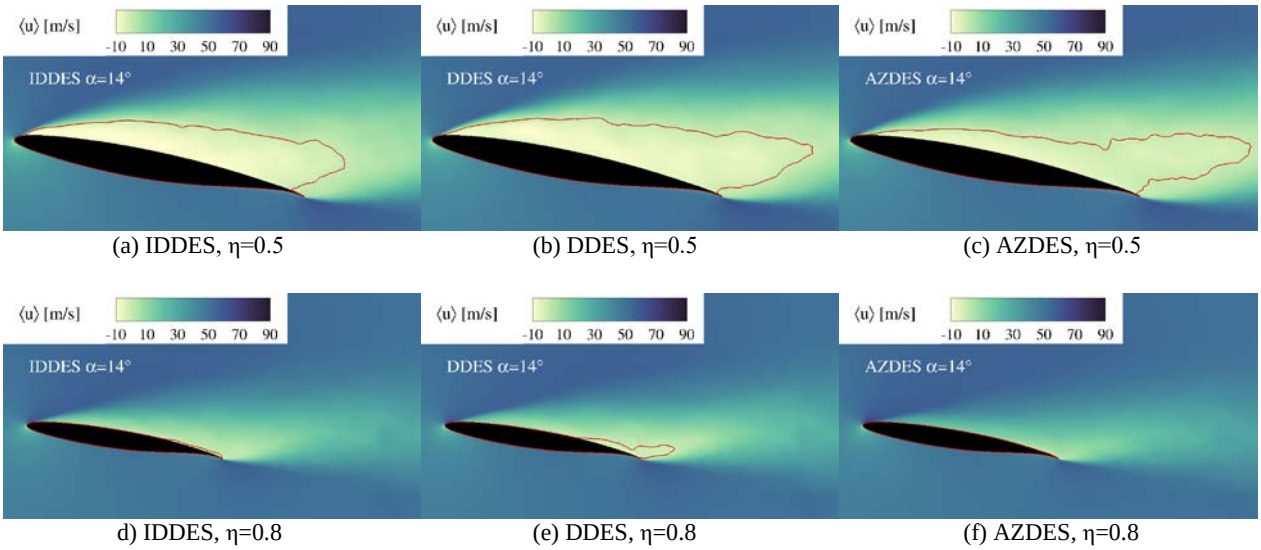

(a) IDDES, η=0.5 (b) DDES, η=0.5 (c) AZDES, η=0.5

d) IDDES, η=0.8 (e) DDES, η=0.8 (f) AZDES, η=0.8

Figure 3-10: Time averaged streamwise velocity at α=14° in two slices though the CRM wing. The red line represents ⟨u⟩=0 m/s.

4.0 CONCLUSIONS

In the present work a computational study of low speed stall of the CRM at moderate angles of attack was conducted. A comparison of different hybrid RANS/LES models and experimental data showed that all models tend to overestimate the extent of separated flow at beginning wing stall. While AZDES and DDES lead to a similar separation characteristic with a large area of separated flow in the outer region of the wing at α=12°, IDDES yields a smaller separation area and is in better agreement with the experiment between 28% and 85% halfspan at this angle of attack. This different behavior might be traced back to a difference in the filter width definition of the models, where IDDES leads to the development of small scale turbulent structures and their accelerated breakup. Simulations at α=14° showed similar results for all three models in terms of the spanwise extent of flow separation and mean pressure distribution. At this angle of attack, IDDES also showed smaller turbulent structures and an overall smaller extent of the recirculation area over the wing surface. For future investigations, different turbulence models will be applied as well as a refinement of the grid in the leading edge area, as this region seems to limit the early resolution of turbulence. A further acceleration from RANS to LES might be achieved by reducing the dissipation in RANS areas.

5.0 ACKNOWLEDGEMENTS

The work is funded by the German Research Association (DFG) in the project LU 809/8. Furthermore, the authors gratefully acknowledge DLR for providing the TAU source code. We would also like to thank the High Performance Computing Center Stuttgart (HLRS) for the support and the computational resources. The simulations were performed on the CRAY XC40 (Hazel Hen), which is funded by the Federal Ministry of Education and Research and the Ministry of Higher Education, Research and Arts Baden-Württemberg.

6.0 REFERENCES

[1] Deck S. “Zonal Detached Eddy Simulation of the Flow Around a High-Lift Configuration.” AIAA Journal 43(11):2372–23 (2005)

[2] Ehrle, M. C.; Waldmann, A.; Lutz, T.; Krämer, E. “An Automated Zonal Detached Eddy Simulation Method for Transonic Buffet.“ Contribution to the 7th symposium of hybrid RANS-LES methods (2018); accepted for publication.

[3] Harper, C. W., & Maki, R. L. “A Review of the Stall Characteristics of Swept Wings.” NASA Technical Note TN D-2373 (1964).

[4] Huang, R.F., Lin, C.L.: “Vortex Shedding and Shear-Layer Instability of Wing at Low Reynolds Numbers.” AIAA Journal **33**(8), 1398–1403 (1995)

[5] Illi, S., Fingskes, C., Lutz, T., Krämer, E.: Transonic Tail Buffet Simulations for the Common Research Model (2013). https://doi.org/https://doi.org/10.2514/6.20132510, AIAA 2013-2510

[6] Kok, J.:“A High-Order Low-Dispersion Symmetry-Preserving Finite-Volume Method for Compressible Flow on Curvilinear Grids.” J. Comp. Phys 228(18), 6811–6832 (2009)

[7] Luckring, J. “A Survey of Factors Affecting Blunt-Leading-Edge Separation for Swept and Semi-Slender Wings.” In 28th AIAA applied aerodynamics conference (p. 4820) (2010).

[8] Lutz, T., Gansel, P.P., Waldmann, A., Zimmermann, D.M., Schulte am Hülse, S.A.: “Time-Resolved Prediction and Measurement of the Wake past the CRM at High Reynolds Number Stall Conditions.”

Journal of Aircraft 53(2), 501–514 (2016). https://doi.org/10.2514/1.C033351

[9] Mockett, C., Fuchs, M., Garbaruk, A., Shur, M., Spalart, P., Strelets, M., Thiele, F., Travin, A.: "Two Non-Zonal Approaches to Accelerate RANS to LES Transition of Free Shear Layers in DES." In: Girimaji, S., Haase, W., Peng, S.H., Schwamborn, D. (eds.) Progress in Hybrid RANS–LES Modelling. Notes on Numerical Fluid Mechanics and Multidisciplinary Design, vol. 130, pp.187–201. Springer (2015)

[10] Probst, A., Schwamborn, D., Garbaruk, A., Guseva, E., Shur, M., Strelets, M., Travin, A.: "Evaluation of Grey Area Mitigation Tools within Zonal and Non-Zonal RANS-LES Approaches in Flows with Pressure Induced Separation." International Journal of Heat and Fluid Flow 68, 237–247 (2017)

[11] Schwamborn, D., Gerhold, T., Heinrich, R.: "The DLR TAU-Code, Recent Applications in Research and Industry." European Conference on Computational Fluid Dynamics ECCOMAS CFD 2006 (Sep 2006)

[12] Shur, M. L., Spalart, P. R., Strelets, M. K., & Travin, A. K. (2008). "A Hybrid RANS-LES Approach with Delayed-DES and Wall-modelled LES Capabilities." International Journal of Heat and Fluid Flow, 29(6), 1638-1649.

[13] Spalart, P.R., Jou, W.H., Strelets, M., Allmaras, S.: "Comments on the Feasibility of LES for Wings, and on a Hybrid RANS/LES Approach." In: Mockett, C., Haase, W., Schwamborn, D. (eds.) Advances in DNS/LES: proceedings of the First AFOSR International Conference on DNS/LES. pp. 137–148. Greyden Press, Columbus, OH (1997)

[14] Spalart, P.R., Deck, S., Shur, M.L., Squires, K.D., Strelets, M.K., Travin, A.: "A New Version of Detached-Eddy Simulation, Resistant to Ambiguous Grid Densities." Theoretical and Computational Fluid Dynamics20(3), 181–195 (2006)

[15] Vassberg, J.C., DeHaan, M.A., Rivers, M.B., Wahls, R.A.: "Development of a Common Research Model for Applied CFD Validation Studies" (Aug 2008) , https://doi.org/10.2514/6.2008-6919,AIAA 2008-6919

[16] Waldmann, A., Gansel, P.P., Lutz, T., Krämer, E.: "Unsteady Wake of the NASA Common Research Model in Low-Speed Stall." Journal of Aircraft **53**(4), 1073–1086 (2016). https://doi.org/10.2514/1.C033413

[17] Waldmann, A., Lutz, T., and Krämer, E., "Unsteady Simulation of a Separated Wake of a Transport Aircraft by Detached Eddy Simulation," New Results in Numerical and Experimental Fluid Mechanics XI, Springer International Publishing, Cham, 2017, pp. 61–71.